Semiclassical magnetotransport theory for two-dimensional electron systems in lateral superlattices

J. Kučera* and P. Středa
Institute of Physics, CZ-162 00 Praha, Czech Republic

R. R. Gerhardts
Max-Planck-Institut für Festkörperforschung, D-7000 Stuttgart 80, Germany

(Received 9 August 1996)

Based on the correct single-electron energy spectra we calculate, within a semiclassical approach, the conductivity of periodically modulated two-dimensional electron systems in a perpendicular magnetic field B. For $B=0$ we obtain, as a function of the Fermi energy, fluctuations of the conductivity, which result from the energy gaps in a perfectly periodic modulation potential, but may easily be smeared out by disorder. Introducing a smooth interpolation between the energy bands in the extended zone scheme and taking magnetic breakdown effects properly into account, we calculate the magnetoresistance for a strong unidirectional modulation and magnetic fields of arbitrary strengths, neglecting these quantum fluctuations.
[S0163-1829(97)07521-8]

I. INTRODUCTION

The modern techniques of microstructuring allow preparation of a new class of materials, the lateral superlattices. In low magnetic fields applied perpendicularly to these two-dimensional systems peculiar transport properties are observed.[1] Except for the well-known magnetoresistance oscillations due to the commensurability effects,[2–5] a number of low field magnetoresistance anomalies appear at low temperatures.

A typical, often observed anomaly is a positive magnetoresistance followed by a resistance drop at higher magnetic fields.[2–5] Such behavior was observed on metallic single crystals.[6,7] It has been successfully explained by the suppression of Bragg reflections due to the Lorenz force induced by magnetic fields, an effect known as magnetic breakdown.[8] A pronounced negative magnetoresistance has also been observed, usually in strongly modulated two-dimensional systems, e.g., in the case of unidirectional modulation[9] and in a lattice of antidots.[10,11] To understand these low-field magnetoresistance anomalies a semiclassical description is usually satisfactory. It is based on the knowledge of the velocity distribution of Fermi electrons at zero magnetic field which is controlled by parameters of the potential modulation.

The artificial crystals have quite a large lattice constant, usually of the order of several hundreds of nanometers. The effect of the underlying natural crystalline potential may thus be included by introducing the effective electron mass m^* into the kinetic energy, and single-electron properties are controlled by the Hamiltonian

$$H=\frac{p_x^2}{2m^*}+\frac{p_y^2}{2m^*}+V(x,y), \tag{1}$$

where $V(x,y)$ stands for a periodic potential modulation. The eigenfunctions are of the Bloch type, with the wave vector $\vec{k}$ being a good quantum number. In standard artificial superlattices there are usually many electrons within the unit cell and the lattice constant is much larger than the Fermi wavelength λ_F defined by the average carrier density n_s of the two-dimensional electron gas, $2\pi/\lambda_F=\sqrt{2\pi n_s}$. Opposite to the natural single crystals, many Brillouin zones are occupied and the energy $E(\vec{k})$ of most of the electrons will be close to the free electron one. The extended zone scheme thus seems to be convenient for the description of energy dispersions.

The discontinuities of the energy dispersion $E(\vec{k})$ along a particular direction, which appear at the Brillouin zone boundaries, are essentially of two distinct origins. First, in the energy range in which the classical motion is bounded between the potential wells, wide gaps separate narrow energy bands with eigenfunctions which are mainly localized within the wells and have exponentially decaying tails in the barriers. These discontinuities are essentially due to the size quantization within the potential wells of the periodic potential[12] and affect the momentum distribution significantly if the electron mean free path is larger than the lattice period, a condition often reached in the experiment. The second type of discontinuities originates in standard Bragg reflections in the energy range in which the classical motion is not confined to a single period of the superlattice. Here the interference of partial waves scattered from different reflection planes leads to narrow gaps between broad energy bands of extended wave functions with considerable amplitude between the wells. These gaps due to interference can easily be smeared out by imperfect periodicity, but in the ideal case they may strongly influence the conductivity.

The characteristic features of one-dimensional energy dispersion will be summarized in Sec. II. The following Sec. III will be devoted to the description of Fermi surfaces for the cases of the unidirectional modulations and bidirectional modulations of square symmetry. For the sake of simplicity a separable periodic potential has been considered. The calculation has been performed for cosine and Kronig-Penney-like modulations representing weak and strong Bragg reflection

effects, respectively. Both types of potentials lead to an eigenvalue problem which scales with the product a^2V_0, a and V_0 being modulation period and amplitude, respectively, so that the value of the single parameter q,

$$q \equiv \frac{1}{\hbar}\frac{a}{\pi}\sqrt{m^* V_0}, \tag{2}$$

determines the effect of the potential. The results of the precise numerical calculation will be compared with a ''classical approach,'' which smoothly interpolates between the energy bands in the extended zone scheme and eliminates the discontinuities of quantum origin.

Transport phenomena within semiclassical theory are interpreted in terms of the electron distribution function $f(\vec{r},\vec{k})$ which satisfies the Boltzmann equation. We limit our consideration to low temperatures for which the electrons at the Fermi energy determine the transport properties. We will also assume that the equilibration length for electrons is much larger than the lattice constant. In this case the electric field, arising due to the energy dissipation from the current drawn through the sample, may be assumed as spatially uniform and only the $\vec{k}$ dependence of the distribution function needs to be taken into account. Note that in the opposite limit the transport properties are controlled by local Drude conductivities and we are left with a periodic series of resistors, which allows a simple calculation of the average resistance.

To emphasize the effect of electron energy spectra on the conductivity we will assume that the relaxation processes may be described by a uniform relaxation time. In such a case the zero-temperature conductivity is exclusively controlled by velocity expectation values

$$\vec{v}(\vec{k}) = \frac{1}{\hbar}\nabla_{\vec{k}} E(\vec{k}) \tag{3}$$

of the Fermi edge electrons. The obtained conductivity dependences together with the ''classical approach'' will be presented in Sec. IV.

In the presence of a weak magnetic field $\vec{B} \equiv (0,0,B)$ applied perpendicular to the two-dimensional electron gas the dynamics of the electron motion, when treated semiclassically, is governed by the equation of motion:

$$\hbar\frac{\partial \vec{k}}{\partial t} = -e\vec{v}(\vec{k}) \times \vec{B}. \tag{4}$$

The time dependence of wave vector $\vec{k}$ describes an electron motion along states having the same energy. Due to reflections at Brillouin zone boundaries there appears a number of different trajectories. Their topology, especially the ratio of open and close trajectories, controls the main features of the magnetotransport. The above scheme is applicable if the cyclotron energy is much less than the energy gaps. It can, however, be generalized so that it captures much of the additional high-field physics in a physically appealing way. The generalization[8,13] is to acknowledge that electrons approaching Brillouin zone edges have a finite probability for tunneling through the barrier and moving from one trajectory to another. This effect, known as magnetic breakdown, will be discussed in Sec. V. The distinct features of this effect at the Fermi surface discontinuities, resulting from the interference effect and size quantization, will be described.

Low-field magnetoresistance for the case of a unidirectional potential modulation has been studied by different approaches. Main attention has been paid to the explanation of the commensurability effect.[3,14,15] The above-described concept of $\vec{k}$-space electron trajectories has also been applied for the particular case of very weak potential modulation,[16] i.e., to the case with $q \ll 1$. Obtained results have been in qualitative agreement with the experimental observation, i.e., strong positive magnetoresistance approaching a maximum due to the magnetic breakdown and commensurability oscillations at higher magnetic fields. However, the predicted scaling of the magnetoresistance peak positions with the parameters of the potential modulation did not agree with the available experimental data. This suggests that in standard systems the parameter q, defined by Eq. (2), is not much less than 1 and the potential modulation cannot be treated as a weak perturbation.

The proper scaling of magnetoresistance breakdown peaks has been derived by Beton *et al.*[5,17] Using classical arguments they have found a decreasing number of open trajectories with increasing magnetic field strength. For the studied cosine modulation it vanishes if the maximum electric force $2\pi V_0/a$ is equal to the magnetic force eBv_F. However, at the critical magnetic field $B_{\rm crit}$, defined in this way, their model predicts a very rapid fall in the magnetoresistance which is not seen in experiments.

Section VI will be devoted to the magnetoresistance for the case of very strong unidirectional modulation for which the Weiss oscillations are usually not observed. For this reason and for the sake of simplicity, the commensurability effect has been excluded from our consideration. It will be shown that the proper trajectory statistics gives not only the observed scaling of breakdown peak positions but also a pronounced positive magnetoresistance for magnetic fields well above $B_{\rm crit}$.

II. ONE-DIMENSIONAL ENERGY DISPERSION AND THE CLASSICAL LIMIT

The energy spectrum of an electron moving in a one-dimensional channel periodically modulated by a potential $V(x)$ of the period a is one of the standard eigenvalue problems defined by the Hamiltonian

$$H = \frac{p_x^2}{2m^*} + V(x). \tag{5}$$

The result of a numerical calculation for the Kronig-Penney-like potential

$$V^{(\rm KP)}(x) = V_0 \,\mathrm{sgn}\left[\cos\frac{2\pi x}{a}\right] \tag{6}$$

and for the cosine modulation

$$V^{(\cos)}(x) = V_0 \cos\frac{2\pi x}{a} \tag{7}$$

are shown in Fig. 1.

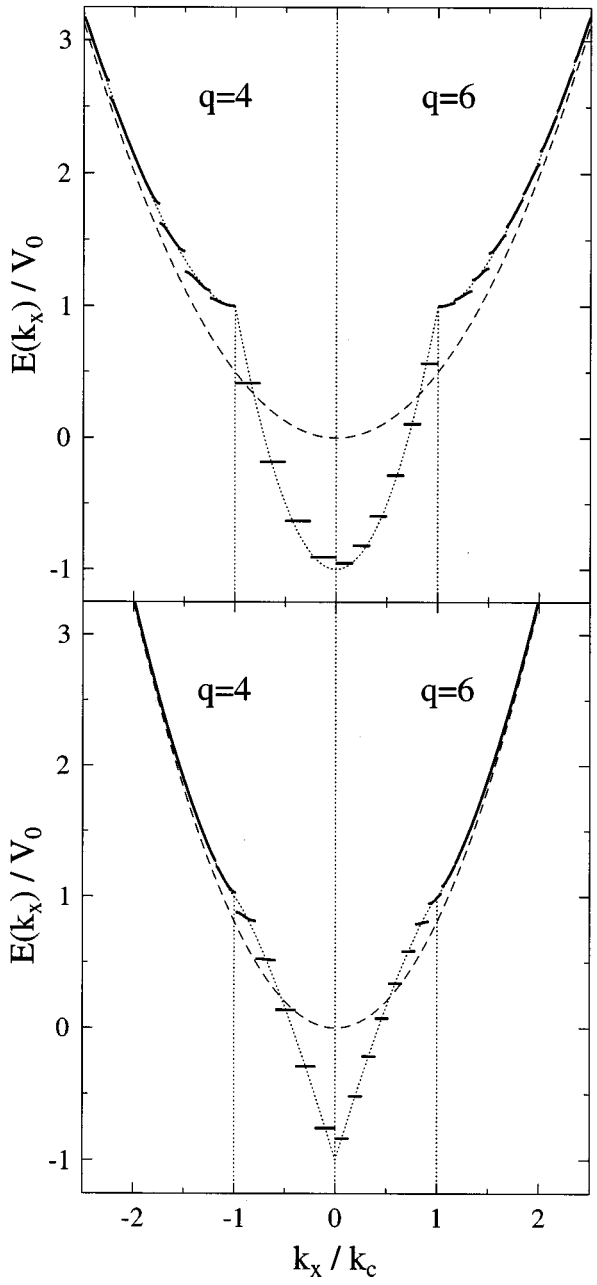

FIG. 1. Energy spectra for a one-dimensional periodically modulated channel with the Kronig-Penney (top) and the cosine (bottom) potential. With increasing the modulation strength ($q=4$ on the left, 6 on the right, respectively) the exact calculation (solid) yields a growing number N_b of states localized below the potential maxima. The dotted lines represent the classical approach and the dashed lines correspond to zero modulation.

Due to the effect of Bragg reflections at Brillouin zone boundaries energy gaps appear and the spectrum is composed of minibands. They will be numbered by the index $i=0,1,2,\ldots$ increasing with miniband energy. The low lying minibands are flat due to the wide energy barriers separating adjacent potential minima and preventing a significant overlap of wave functions. For energies well above V_0 the energy gaps become smaller and the energy dispersion approaches the free electron quadratic dispersion law. The considered eigenvalue problem scales with the parameter q^2 defined by Eq. (2), i.e., with the product a^2V_0. Further, plotting $E(k_x)\cdot a^2$ as a function of k_xa, the miniband positions are approximately lying on the same curve representing the classical limit $a\rightarrow+\infty$.

For the case of the Kronig-Penney-like potential, Eq. (6), an explicit expression for the approximate miniband dispersion may be obtained. According to the Bohr-Sommerfeld quantizing condition, eigenenergies ϵ_i well below V_0 coincide with eigenenergies of a box with hard walls and width $a/2$

$$\epsilon_i^{(\mathrm{KP})}\cong 4\frac{\hbar^2}{2m^*}\left(\frac{i\pi}{a}\right)^2-V_0. \tag{8}$$

There are approximately

$$N_b^{(\mathrm{KP})}\cong\frac{a}{\pi\hbar}\sqrt{m^*V_0}=q \tag{9}$$

narrow bands corresponding to well-localized states within one particular potential well, i.e., below the energy V_0.

Having in mind that the energy spectrum of a large box is only weakly dependent on the applied boundary conditions, the miniband dispersion for higher energies may easily be obtained for large enough values of a. In the regions of the flat potential, electrons may be assumed as free with the density of states per unit length $\sqrt{m^*/2}/(\pi\hbar\sqrt{E\pm V_0})$. For energies E above V_0 the density is given as the sum of both contributions and for the integrated density per one period we get

$$N(E)=\frac{a}{\pi\hbar}\sqrt{\frac{m^*}{2}}(\sqrt{E-V_0}+\sqrt{E+V_0}). \tag{10}$$

Within each miniband there is one state per unit cell, so that $N(E)$ may be identified with the miniband index i. With $k_x=\pi i/a=\pi N(E)/a$, Eq. (10) leads to the following approximation for the miniband dispersion

$$\epsilon_i^{(\mathrm{KP})}\cong E\left(k_x=\frac{\pi i}{a}\right)=\left[4\frac{\hbar^2k_x^2}{2m^*}-V_0\right]\theta(k_c^{(\mathrm{KP})}-|k_x|)+\left[\frac{\hbar^2k_x^2}{2m^*}+\left(\frac{V_0}{2}\right)^2\frac{2m^*}{\hbar^2k_x^2}\right]\theta(|k_x|-k_c^{(\mathrm{KP})}), \tag{11}$$

where k_c is the critical wave number

$$k_c^{(\mathrm{KP})}=\frac{1}{\hbar}\sqrt{m^*V_0} \tag{12}$$

and the function θ equals 1 or zero for positive or negative argument, respectively. This defines our ''classical approach'' to the Kronig-Penney energy spectrum, which is a continuous function of k_x, shown as dotted line in the upper part of Fig. 1.

The above-described classical approach can be generalized for an arbitrary form of the potential by dividing the period a into a number of narrow regions. For the cosine modulation, Eq. (7), we have obtained

$$N_b^{(\cos)}\cong\frac{4}{\pi}q,\quad k_c^{(\cos)}=\frac{4}{\pi}\frac{1}{\hbar}\sqrt{m^*V_0}. \tag{13}$$

As expected, in this case the energy of low lying flat minibands increases linearly with miniband index i due to the parabolic form of local potential minima. The energy dispersions obtained from the limit $a \to +\infty$ quite well approximate results of the precise calculation as shown in Fig. 1.

In both cases the critical wave number k_c divides electronic states into two regions of distinct properties. Values $|k_x| < k_c$ correspond to states well localized within the potential wells and belonging to narrow bands. The corresponding expectation values of the velocity, Eq. (3), essentially vanish. In the ''classical approach'' we shall take $v_x \equiv 0$ for states with $|k_x| < k_c$. All other states represent nearly free electrons with vanishing velocity at Brillouin zone boundaries only, as shown in Fig. 2. The velocity maxima are close to the result of the classical limit which neglects Bragg reflections. For energies well above V_0 they are approaching free electron values supporting the extended zone scheme as a relevant view to the electron transport properties of lateral superlattices. In the ''classical approach'' we shall calculate v_x for $|k_x| > k_c$ from the approximate energy dispersion, e.g., from Eq. (11).

III. FERMI SURFACES

The energy spectra for periodic modulation defined by a separable potential

$$V(x,y) = V(x) + V(y) \tag{14}$$

are given as the sum of one-dimensional dispersions of the Hamiltonian, Eq. (5). For the sake of simplicity only the same modulation along both directions will be considered. The one-dimensional miniband structure is reflected in the topology of the Fermi surface. Within the extended zone scheme it becomes split into a number of segments located between Brillouin zone boundaries. In Fig. 3 the Fermi surfaces for the case of the unidirectional Kronig-Penney-like modulation, Eq. (6), are shown. The cases of a bidirectional modulation are represented by Fermi surfaces shown in Fig. 4 and Fig. 5. As discussed above, for the Fermi energies E_F above V_0, the condition $a \gg \lambda_F$ allows one to divide Fermi electrons into two distinct groups, bounded and nearly free electrons.

In the regions where $|k_x|$ or $|k_y|$ is less than k_c there are flat miniregions arising due to the size quantization within potential wells of which the modulation is composed. Their positions k_α^i $(\alpha = x,y)$ are defined by the following equality:

$$E(k_\alpha^i) = E_F - \epsilon_i , \tag{15}$$

where ϵ_i denotes energy levels of the potential well. In real space, the amplitude of corresponding eigenfunctions vanishes exponentially in a region around potential maxima V_0. The states for which $|k_x|$ as well as $|k_y|$ are less than k_c are bound states. Those states, for which the only one of the conditions ($|k_x| < k_c$ or $|k_y| < k_c$) holds, are bound in one direction only. As the result, quasi-one-dimensional conducting channels at the energies above the potential maxima are formed.

Note that for some values of the Fermi energy the equality Eq. (15) need not be fulfilled for any value of k_α due to the existence of energy gaps in the dispersion $E(k_\alpha)$. This may happen in the case of bidirectional modulation and the corresponding flat minisegment disappears from the Fermi surface, as may be seen in Fig. 4. The occurrence and/or absence of individual segments of the Fermi lines, even for very close values of the Fermi energy, is due to the interplay of the energy gaps in the one-dimensional energy spectra. In the case of a wide gap even several minisections may be missing as shown in Figs. 5 and 6. On the other side the classical approach ignoring gap structure always leads to a continuous Fermi contour.

The rest of the Fermi surface is segmented due to the Bragg reflections only, i.e., due to the interference effects. Electrons in these states are called nearly free electrons since

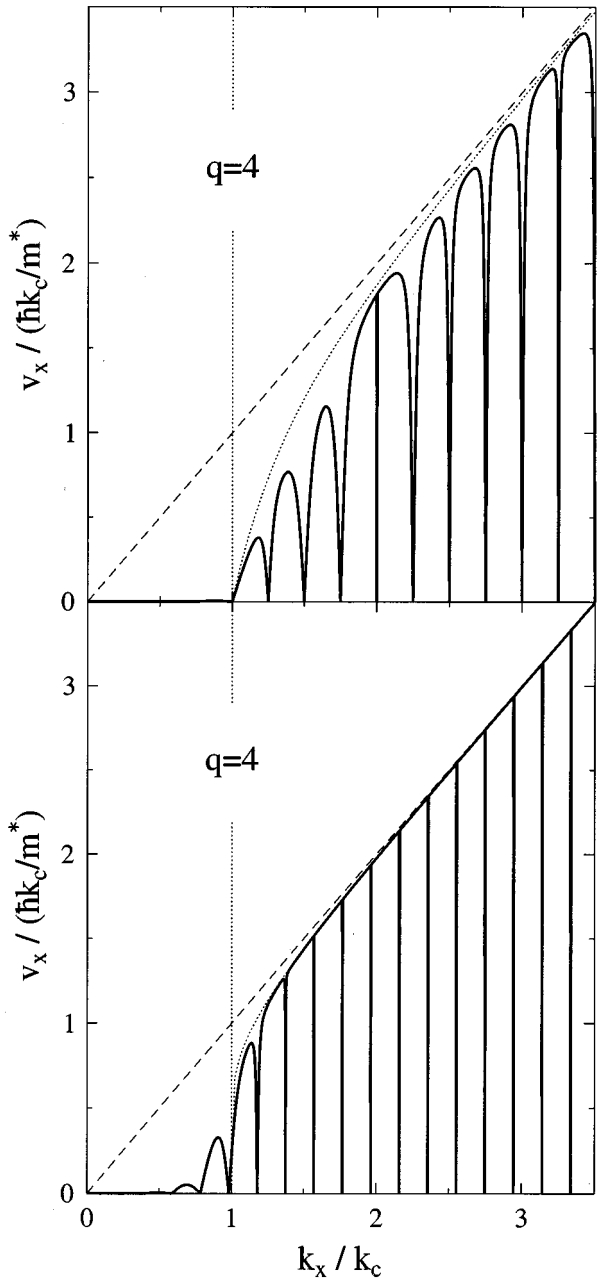

FIG. 2. Mean velocity $v = (1/\hbar)\ dE/dk$ for a one-dimensional periodically modulated channel with the Kronig-Penney (top) and the cosine (bottom) potential. The dotted lines represent the classical approach and the dashed lines correspond to zero modulation.

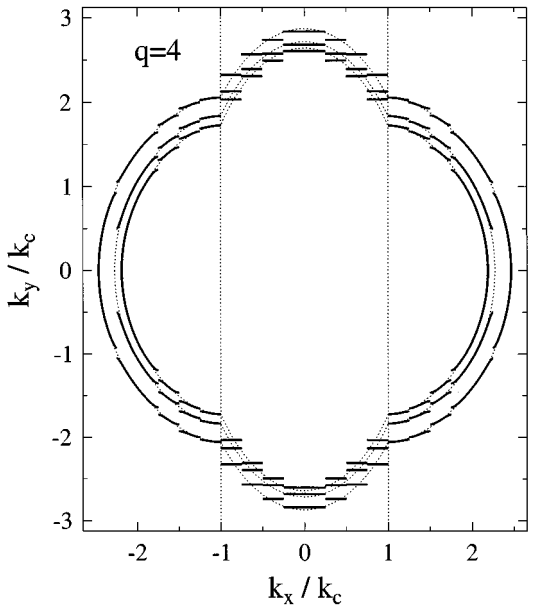

FIG. 3. Fermi lines for unidirectional Kronig-Penney modulation, at $E_F/V_0=2.5$, 2.7, 3.1. Missing states close to $k_y=0$ for $E_F/V_0=2.7$ lead to a dip in the conductivity (cf. Fig. 6).

they can overcome potential maxima of the modulation. Their effective mass is generally larger than m^*.

IV. CONDUCTIVITY

Assuming the elastic scattering as dominant, the linearization of the Boltzmann equation with respect to an external electric field gives the following expression for the conductivity at zero temperature:

$$\sigma_{\alpha\alpha}=\frac{e^2}{2\pi^2}\int \delta[E_F-E(\vec{k})]v_\alpha(\vec{k})\tau v_\alpha(\vec{k})d^2k, \qquad (16)$$

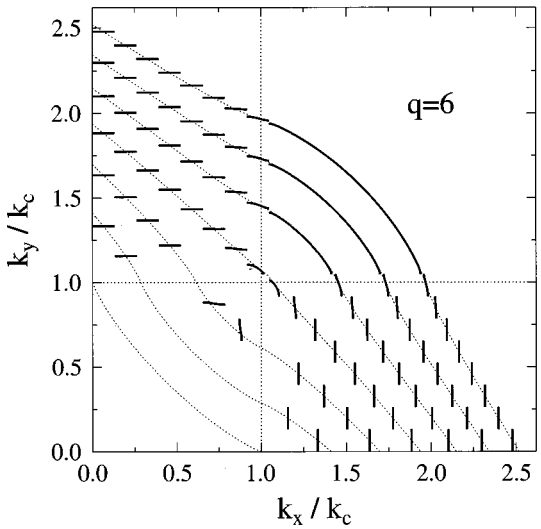

FIG. 4. A series of Fermi lines for the bidirectional cosine modulation at E_F/V_0 = 0, 0.7, 1.4, 2.1, 2.8, 3.5, and 4.2. Results of the classical approach are presented by dotted lines.

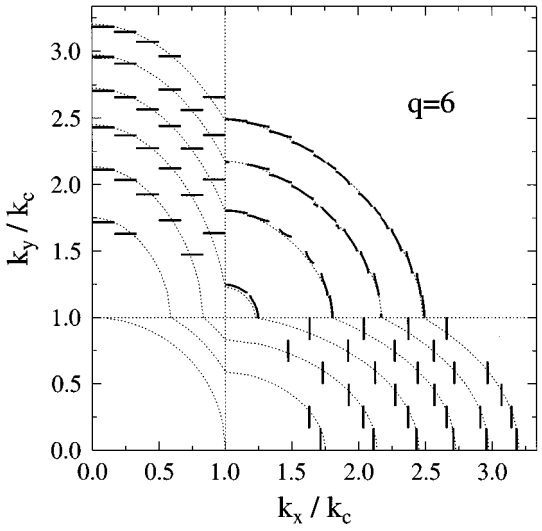

FIG. 5. A series of Fermi lines for the Kronig-Penney bidirectional modulation at $E_F/V_0=0$, 0.7, 1.4, 2.1, 2.8, 3.5, and 4.2. Results of the classical approach are presented by dotted lines.

where τ is the uniform relaxation time. The contribution of bound electrons in states represented by flat minisections of the Fermi surface can be written as the sum of corresponding velocities

$$\sigma_{\alpha\alpha}^{(b)}=\frac{e^2\tau}{m^*}\frac{2m^*}{\pi a\hbar}\sum_{i=0}^{i_{\max}}|v_\alpha(k_\alpha^i)|, \qquad (17)$$

where k_α^i is defined by Eq. (15). It represents the average electron drift.

In addition to the precise numerical calculation the results of the classical limit which neglects energy quantization are also presented in Figs. 7 and 8. In this limit the gap structure is smeared out, nevertheless the states for which $|k_\alpha|<k_c$ remain bound, at least in one direction along which the velocity remains zero (see Fig. 2). To evaluate $\vec{k}$-space inte-

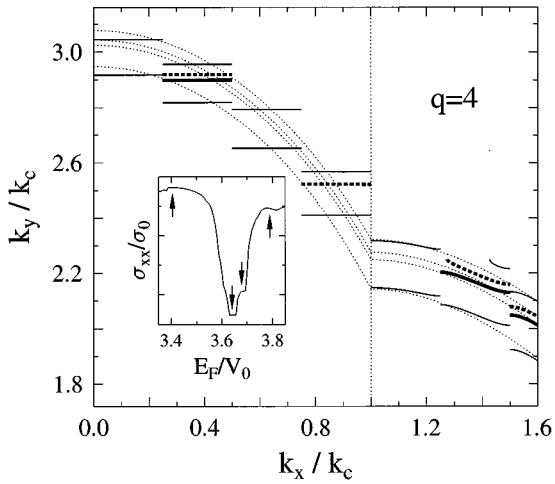

FIG. 6. Detail of the Fermi line scheme for the Kronig-Penney bidirectional modulation, at $E_F/V_0=3.40$ (''inner'' thin solid), 3.63 (thick solid), 3.69 (thick dashed), and 3.79 (''outer'' thin solid). The corresponding conductivity values are indicated by arrows in the inset.

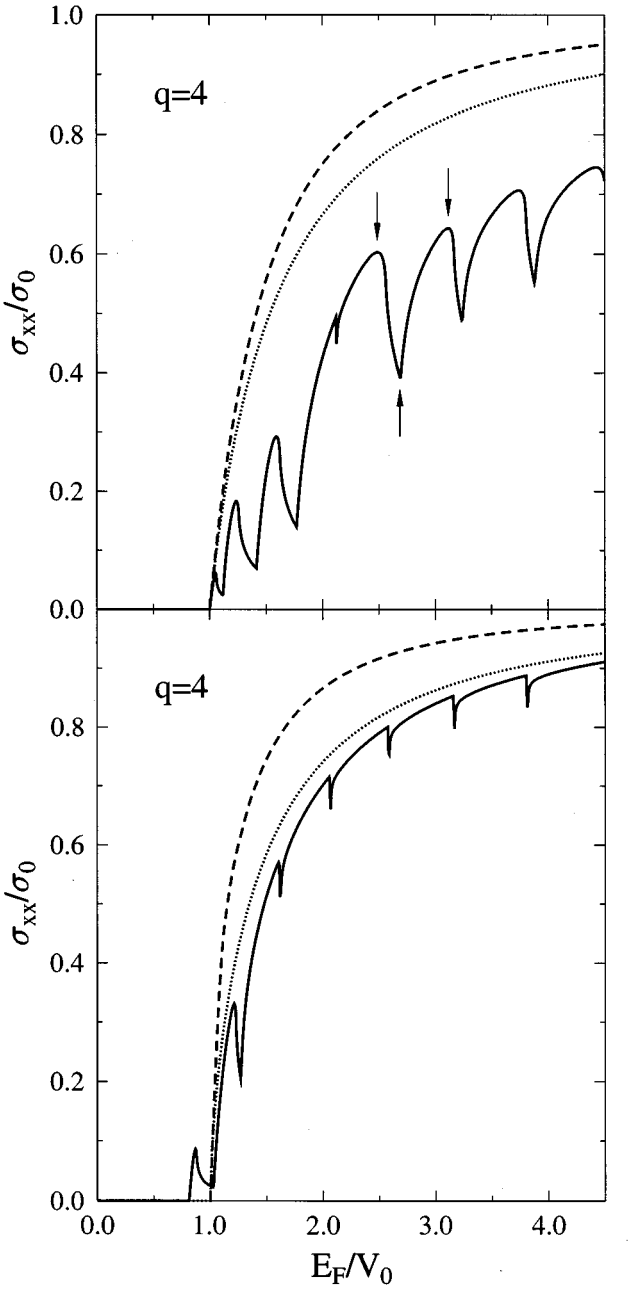

FIG. 7. The conductivity σ_{xx} for the case of unidirectional Kronig-Penney (top) and cosine (bottom) modulation. The classical approximation is presented by dotted lines and the conductivity representing a series of resistors by dashed lines. The arrows indicate the three values of conductivity, corresponding to the Fermi lines depicted in Fig. 3.

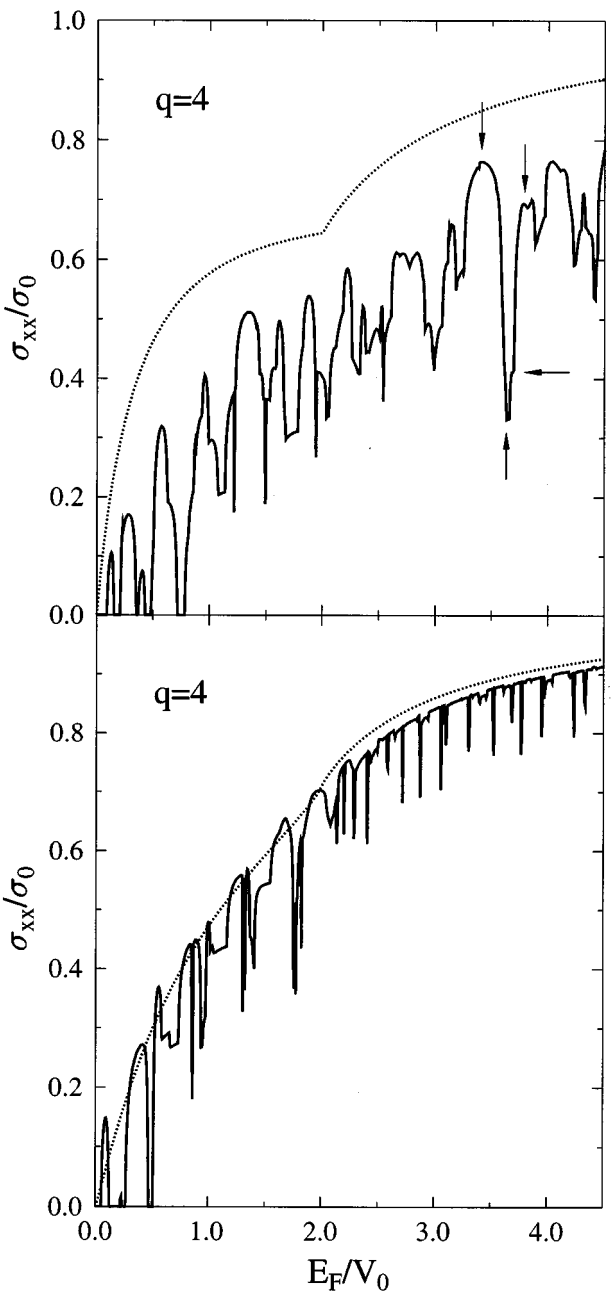

FIG. 8. The conductivity σ_{xx} for the case of bidirectional Kronig-Penney (top) and cosine (bottom) modulation. The classical approximation is presented by dotted lines.

grals like that in Eq. (16) in the classical limit, we integrate over energy and the k component along the lines of constant energy, $d^2k = d\epsilon dk_{\parallel}/(\hbar|\vec{v}(\vec{k})|)$, with $E(\vec{k})=\epsilon$, and take $v_\alpha(\vec{k})=0$ and $dk_{\parallel}=dk_\alpha$ in the region of bounded states, i.e., for $|k_\alpha|<k_c$.

As expected in all cases the classical conductivity is larger than that with the interference effects taken into account. The conductivity resulting from modeling the periodic potential as a series of resistors is even higher, as shown in Fig. 7 by dashed lines. The fact that the difference between the exact calculation and the classical approach is larger for the Kronig-Penney model than for the case of the cosine potential, corresponds to the more important role of the Bragg reflections in the former case.

A. Unidirectional modulation

Assuming a periodic modulation in the $\hat{x}$ direction the energy of electron motion along the $\hat{y}$ direction is purely kinetic and the energy dispersion is given as

$$E(\vec{k}) = E(k_x) + \frac{\hbar^2 k_y^2}{2m^*}. \tag{18}$$

The electrons bounded in the $\hat{x}$ direction contribute to the yy component of the conductivity only, and inserting explicit velocity values into Eq. (17) we get

$$\sigma_{yy}^{(b)}=\frac{e^2\tau}{m^*}2\sum_{i=0}^{i_{\max}}\frac{|k_y^i(E_F)|}{\pi a}\cong\sigma_0\frac{n_s^{(b)}}{n_s}, \tag{19}$$

where $n_s^{(b)}$ is the areal density of bound electrons (number of bound states with energy $E\leqslant E_F$, per area), n_s is the total electron density, and $\sigma_0=e^2\tau n_s/m^*$ is the free electron conductivity. The second part of Eq. (19) is seen if in the $\vec{k}$-space integral defining the integrated density of states $n_s^{(b)}(E_F)$ the energy integral is evaluated first. The rest of electrons, which are nearly free, contributes to both components of the conductivity. Note that, since there is no effect of the modulation on the electron mass in the $\hat{y}$ direction, it can be generally proved that the total conductivity component σ_{yy} is just equal to σ_0.

In Fig. 7 the results of the numerical calculation are shown. Deep local minima in the energy dependence of σ_{xx} appear whenever there exists a discontinuity of the Fermi surface just at the k_x axis where maximum velocity expectation values $v_x(\vec{k})$ are expected. The distance between adjacent dips thus approximately scales with the parameter q as

$$\frac{\Delta E_F}{V_0}\cong\frac{\sqrt{2}}{q}\sqrt{\frac{E_F}{V_0}}. \tag{20}$$

For the Kronig-Penney model with the classical approximation (11), the integral (16) can be evaluated analytically with the result

$$\frac{\sigma_{xx}^{(\text{class})}}{\sigma_0}=1-\frac{3E_F-V_0}{\pi E_F}\sqrt{\frac{E_F-V_0}{2V_0}}+\frac{3E_F^2-2E_FV_0-5V_0^2}{2\pi E_FV_0}\times\arccos\sqrt{\frac{E_F-V_0}{E_F+V_0}}, \tag{21}$$

which is plotted as dotted line in the upper part of Fig. 7 to indicate the scaling of the conductivity with the modulation amplitude. In the limit $V_0\ll E_F$, Eq. (21) yields

$$\frac{\sigma_{xx}^{(\text{class})}}{\sigma_0}\to1-\frac{\sqrt{2}}{\pi}\frac{32}{15}\left(\frac{V_0}{E_F}\right)^{3/2}. \tag{22}$$

The same result can also be obtained from a strictly classical calculation evaluating σ_{xx} from the average drift velocity along the classical trajectories.[18] Note that, for $V_0\ll E_F$, the V_0 dependence of $\sigma_{xx}^{(\text{class})}$ is very different from the result $\sigma_{xx}^{(\text{series})}/\sigma_0=1-(V_0/E_F)^2$ obtained in the local limit for a series of resistors with density $n(x)=n_0[1-V^{(\text{KP})}(x)/E_F]$ (dashed line in the upper part of Fig. 7).

The integrated density of states $n_s^{(b)}(E_F)$ can also be calculated analytically for the Kronig-Penney model in the classical limit. For $-V_0<E_F<V_0$ the result is $n_s^{(b)}(E_F)=(E_F+V_0)D_0/2$, with $D_0=m^*/(\pi\hbar^2)$ the density of states of the unmodulated two-dimensional electron gas. Thus, the density of states in the region of bound states is only $D_0/2$, but the total number of states below $E=V_0$ is the same as for the unmodulated 2DEG. For $E_F>V_0$, one obtains

$$\frac{n_s^{(b)}}{n_s}\cong\frac{1}{\pi E_F}\left[\sqrt{2V_0(E_F-V_0)}+(E_F+V_0)\arcsin\sqrt{\frac{2V_0}{E_F+V_0}}\right], \tag{23}$$

where $n_s=E_FD_0$ is the total density of electrons, including those in unbounded states. For $E>V_0$ the total density of states is D_0, as in the unmodulated 2DEG.

B. Bidirectional modulation

The representative results of the numerical calculations are shown in Fig. 8. For both types of the potential there appear dips in the conductivity dependences on the Fermi energy. For the cosine potential the pronounced dips are limited to the antidot region, i.e., when $E_F<2V_0$. These dips always occur when some of the flat minisegments of the Fermi surface are missing. This is demonstrated in Fig. 6 where Fermi surfaces corresponding to different conductivity values are shown. The average period of the conductivity fluctuation thus scales with the parameter q, as in the case of unidirectional modulation, Eq. (20).

The conductivity contribution due to one of the flat minisections may be estimated with the help of Eq. (19), and we get

$$\frac{\Delta\sigma_{\alpha\alpha}}{\sigma_0}\cong\frac{\sqrt{2}}{q}\sqrt{\frac{V_0}{E_F}}. \tag{24}$$

It gives an estimate for scaling of the fluctuation amplitude with the parameter q. This scaling relation, which may be not quite well seen from the presented results, has been confirmed by a calculation performed for $q=6$ (not shown here).

V. MAGNETIC BREAKDOWN

In the presence of a weak magnetic field B perpendicular to the two-dimensional electron gas the dynamics of the electron motion, when treated semiclassically, is governed by the equation of motion, Eq. (4). Electrons move along $\vec{k}$-space trajectories defined by constant-energy contours. For the transport properties at low temperatures only trajectories at energies close to the Fermi energy are decisive. Their topology dominates the magnetoresistance effects.

Energy spectra $E_i(\vec{k})$ are periodic in $\vec{k}$ space with the period of the reciprocal lattice and at Brillouin zone edges electrons suffer Bragg reflection, i.e., the electron moves along states belonging to one particular miniband. This is the origin of open trajectories for nearly free electron minibands. A special type of open trajectory, quasi-one-dimensional channels, appears due to flat Fermi surface minisegments. It is well known[8] that the existence of open trajectories leads to a positive magnetoresistance $\rho_{\alpha\alpha}\sim B^2$.

However, the applied magnetic field does not only change the electron dynamics, but electron energy spectra are affected as well. The wave vector $\vec{k}$ is no longer a good quantum number. To include this fact, at least partly, the concept of electron trajectories has to be improved by allowing the electron approaching a Brillouin zone edge to have a finite

probability P to tunnel through the relevant Fermi contour discontinuities. The resulting suppression of electron reflections by magnetic fields, known as magnetic breakdown, changes the topology of electron trajectories and has a drastic effect on the electronic transport. Breakdown of open trajectories leads to a suppression of the positive magnetoresistance.

The idea outlined above has been applied in order to describe low-field magnetoresistance of metallic single crystals. It has been found that the tunneling probability, often called the breakdown probability, increases with magnetic field strength, $P \cong \exp(-B_{\rm crit}/B)$. The critical magnetic field $B_{\rm crit}$ is the field for which the reflection is substantially suppressed and the corresponding discontinuity of the Fermi contour becomes effectively closed. It has been calculated using perturbation theory by several authors.[8,13] It has been done in the low-field limit, where it essentially reduces to the theory of Zener electric breakdown, in the high-field limit, where the lattice potential can be treated as a perturbation, and at intermediate fields. In all cases the same formula is obtained

$$B_{\rm crit}^{(Q)}(i) = \frac{\pi}{4} \frac{E_g^2(i)}{e\hbar |\vec{v}^f(i)|^2}, \tag{25}$$

where $\vec{v}^f(i)$ denotes the free electron velocity at the point where the ith Brillouin zone edge crosses the Fermi surface. All these derivations were based on the assumption that the corresponding energy gap $E_g(i)$ is much smaller than the width of surrounding energy bands. Expression (25) is thus applicable to the nearly free electron part of the Fermi contour and the breakdown effect describes a quantum tunneling induced by the magnetic field.

The above result is, however, not applicable to the Fermi contour region composed of flat minisections. Wave functions of these states are quite well localized within regions of potential wells and one of the velocity components vanishes. Quantum tunneling through a barrier between adjacent potential minima is forbidden. Assuming an unidirectional potential modulation along the $\hat{x}$ direction, the energy gap at the particular Brillouin zone edge is just equal to the difference of kinetic energies of Fermi electrons belonging to adjacent minisections,

$$E_g(i) = \epsilon_{i+1} - \epsilon_i = \tfrac{1}{2} m[v_y^2(k_y^i) - v_y^2(k_y^{i+1})] \cong v_y^i \hbar \Delta k_y^i, \tag{26}$$

where $v_y(k_y^i) = v_y^i = \hbar k_y^i / m^*$. In the presence of magnetic fields eigenfunctions can be viewed as a wave packet composed of plane waves with different momenta $\hbar k_y$. If the effective wave packet width $\Delta k_y^i(B)$ becomes comparable with Δk_y^i defined by Eq. (26) the corresponding discontinuity may be assumed as closed. Their equality will be used to define the critical magnetic field.

To estimate the effective wave packet width let us adopt the classical view to the simplest case of the unidirectional Kronig-Penney-like modulation. In the zero-field limit the bounded electron of the velocity expectation value v_y^i can be characterized by the classical electron moving along straight lines with the velocity $v_F^{(b)} = \sqrt{2(E_F + V_0)/m^*}$. It is reflected by potential walls which ensure its localization in the $\hat{x}$ direction within the particular strip of width $a/2$, between right and left reflection points at x_R and x_L, respectively. The slope of the trajectory with respect to the x axis is defined by the value of v_y^i. In the presence of the magnetic force $e\vec{B} \times \vec{v}$ the electron path between reflection points at x_L and x_R becomes circular with the radius R_c controlled by the cyclotron frequency $\omega_c = eB/m^*$, $R_c = v_F^{(b)}/\omega_c$. The velocity component along the $\hat{y}$ direction is changing its value along the trajectory. In weak magnetic fields, when $R_c > a$, the velocity range $\Delta v_y = v_F^{(b)}(x_L/R_c - x_R/R_c)$ is just equal to $a\omega_c/2$. The obtained value $\Delta k_y = m^* \Delta v_y/\hbar = m^* \omega_c a/2\hbar$ can be identified with the effective wave packet width.

To allow an electron in the ith quasi-one-dimensional channel to overcome the potential barrier, the energy ϵ_{i+1} entering Eq. (26) has to be replaced by V_0. The resulting critical magnetic field is given as follows:

$$B_{\rm crit}^{(C)}(i) \cong \frac{2}{ea} \frac{V_0 - \epsilon_i}{|v_y^i|}. \tag{27}$$

This simple geometrical consideration leads to the conclusion that $B_{\rm crit}^{(C)}(i)$ is the magnetic field for which approximately half of the originally bound electrons with $|k_y| < |k_y^i|$ may enter the nearly free electron part of the Fermi contour.

The scaling of critical magnetic fields defined by Eq. (25) and Eq. (27) with the parameters of the periodic potential differs substantially. In the case of the magnetic breakdown in the nearly free electron part of the Fermi contour $B_{\rm crit}^{(Q)} \sim a V_G^2$, with V_G being the relevant Fourier component of the potential. The proportionality to the square of V_G is typical for perturbation theories. For quasi-one dimensional channels $B_{\rm crit}^{(C)}$ scales with the ratio V_0/a as has already been shown by using slightly different definition of the critical magnetic field.[17] Obviously $B_{\rm crit}^{(C)}(i=0) \cong (2/ev_F)(V_0/a)$ for $V_0 \ll E_F$, i.e., the Lorentz force $ev_F B_{\rm crit}^{(C)}$ becomes comparable with the mean electric force $4V_0/a$.

In general, the magnetic breakdown effects describe a gradual transition of the zero-field velocity distribution of Fermi electrons into the distribution given by the classical approach, which neglects interference effects (Bragg reflections) and the size quantization within local potential minima.

VI. MAGNETORESISTANCE OF UNIDIRECTIONALLY MODULATED SYSTEMS

Assuming a uniform relaxation time, we can generalize the expression for the conductivity, Eq. (16), following Chambers,[19] to the case of nonzero magnetic field,

$$\sigma_{\alpha\beta} = \frac{e^2}{2\pi^2} \int \delta[E_F - E(\vec{k})] v_\alpha(\vec{k}, t_0) \times \int_{-\infty}^{t_0} v_\beta(\vec{k}, t) \exp[(t - t_0)/\tau] dt d^2k, \tag{28}$$

where $\vec{v}(\vec{k}, t)$ is the time dependent velocity for the trajectory of an electron which at time t_0 is in the state defined by wave vector $\vec{k}$.

Expression (28) together with the magnetic breakdown concept outlined in the preceding section has already been used to describe magnetoresistance for the case of very weak periodic potential modulation.[16] To describe the main features of the low-field magnetoresistance for the case of a strong modulation, $q \geq 1$, we consider the Kronig-Penney-like periodic potential applied along the $\hat{x}$ direction. We neglect all interference effects and size quantization, i.e., we use the ''classical approach'' to the energy dispersion as described in Sec. II. The corresponding Fermi contour is shown in Fig. 3 by a dotted line. Contour segments of states bounded in $\hat{x}$ direction, $|k_x| < k_c$ with $k_c = \sqrt{m^* V_0}/\hbar$, are defined by the equality

$$E_F = 4\frac{\hbar^2 k_x^2}{2m^*} + \frac{\hbar^2 k_y^2}{2m^*} - V_0 \tag{29}$$

as follows from Eq. (11). Note that the corresponding electron states are localized within a single potential well of the considered Kronig-Penney modulation. This implies that the average value of the velocity component v_x must vanish as well as the expectation value $v_x(\vec{k})$ in the quantum case while $v_y = \hbar k_y / m^*$.

To determine the conductivity, the time integration along the Fermi contour entering Eq. (28) has to be evaluated first. For contour segments with $|k_x| > k_c$ the time dependence of the velocity is quite well defined by the equation of motion, Eq. (4). Let us consider an electron which appears in the state with $k_x = -k_c$ and $k_y > 0$, assuming clockwise motion along the Fermi contour shown in Fig. 3. In the spirit of the magnetic breakdown concept this electron will not be directly reflected into the state with $k_x = k_c$ but it may move along the Fermi segment of bound states and it may eventually suffer the reflection $k_x \rightarrow -k_x$ at a state with $|k_x| \equiv k_x^r < k_c$. Note that the motion along bound states is controlled by electron transitions between minibands, i.e., by the magnetic breakdown effect which, in our ''classical approach,'' may occur at any k_x with $|k_x| < k_c$. To describe electron motion along this part of the Fermi contour, we shall use real-space trajectories of a classical electron within potential well regions.

The Fermi electron at the state with $k_x = -k_c$ and $k_y > 0$ has zero expectation value of the velocity in $\hat{x}$ direction, while the y component has a nonzero value v_y^c. It can be represented by a classical electron having Fermi velocity $v_F^{(b)} = \sqrt{2(E_F + V_0)/m^*}$ and velocity v_y^c along $\hat{y}$ direction. Together with its real-space coordinate (x_0, y_0) within a potential well the subsequent classical motion is well defined, as shown in Fig. 9. The electron moves along the circular path of the radius $R_c = v_F^{(b)}/\omega_c$ with gradually increasing v_y until a value $v_y^r(B, x_0) = v_F^{(b)} \cos\theta_r$ reached at the potential well boundary located at x_L. For given (x_0, y_0) the described real-space path uniquely defines the time evolution of the velocity component $v_y = \hbar k_y / m^*$ and via the identity Eq. (29) the reflection point $k_x^r(B, x_0)$ in $\vec{k}$ space. Note that in zero magnetic field $k_x^r(B, x_0)$ equals to k_c.

It may be expected that, due to the quantum interference, the classical $\vec{r}$-space path, having a crossing point x_c, splits into two parts, the close orbit and a set of bounded states (to the right of x_c) as shown in Fig. 9. Electrons overcoming barriers of the potential modulation are exclusively forming close orbits. In general, they are subjected to the quantum condition expecting an integer number of flux quanta within the area surrounded by the orbit, which determines the allowed values of x_0.

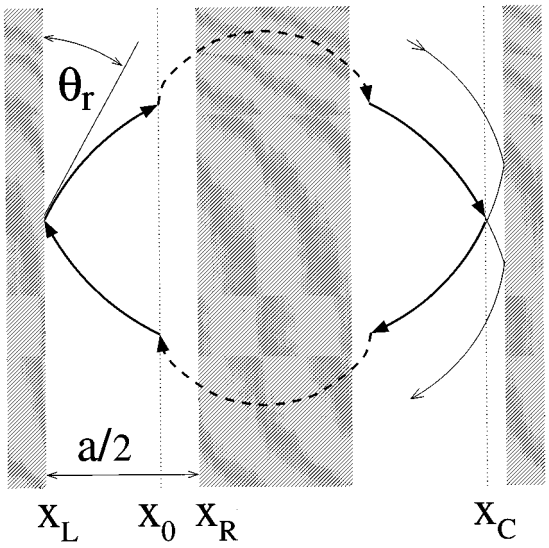

FIG. 9. The close real-space electron orbit is sketched by thick lines. The dashed lines represent the average real-space paths corresponding to the Fermi contour segments with $|k_x| > k_c$. They have been obtained by multiplying $\vec{k}$-space trajectories by a square of the magnetic length and rotated by $\pi/2$. Full lines represent paths of the classical electron within the potential well region. Shadowy areas represent local potential barriers of the Kronig-Penney modulation.

Electrons moving on close orbits in $\vec{r}$ space are periodically returning back into the point (x_0, y_0). This corresponds to the $\vec{k}$-space orbit with reflections $k_x \rightarrow -k_x$ whenever $|k_x| = k_x^r(B, x_0)$. The corresponding contribution to the conductivity is given by the following contour integral:

$$\sigma_{\alpha\beta}^{\text{close}} = \frac{e^2}{2\pi^2} \left\langle \oint_{|k_x| > k_x^r} v_\alpha(\vec{k}, t_0) \int_{-\infty}^{t_0} v_\beta(\vec{k}, t) \times \exp[(t - t_0)/\tau] dt \right\rangle_{x_0} \frac{k\, d\phi}{|\nabla_{\vec{k}} E(\vec{k})|}, \tag{30}$$

where angular brackets denote averaging over all allowed values of x_0. For the sake of simplicity we have assumed that electrons may exceed the critical velocity v_y^c at any position $x_0 \in (x_L, x_R)$ within the well region with the same probability. This assumption excludes commensurability effects as well as magnetic quantization effects from our consideration. Consequently, corresponding Weiss and Shubnikov–de Haas oscillations will be averaged out.

The electrons which do not take part in any close orbit remain bounded within potential wells. Having zero average velocity along the $\hat{x}$ direction, they contribute to σ_{yy} only. It represents a drift velocity and from Eq. (19) we get

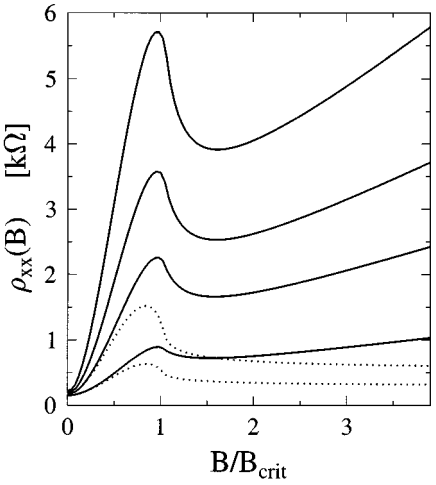

FIG. 10. Magnetoresistance for the case of unidirectional modulation with the period $a=400$ nm for different potential amplitudes. From the top $V_0=5$, 4.5, 4, and 3 meV, respectively. The Fermi energy is 8 meV and $\tau=8$ ps. Dotted lines represent the approach done by Beton *et al.* (Ref. 5) for $V_0=4$ and 3 meV.

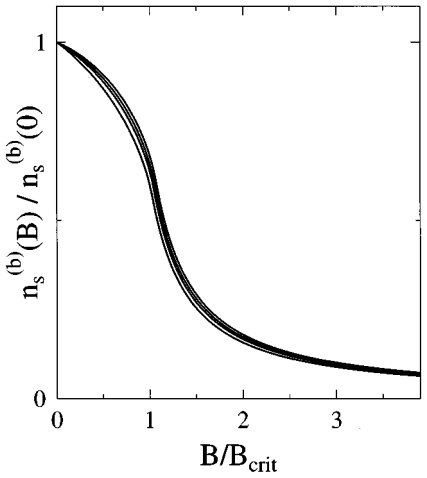

FIG. 11. A relative number of bounded electrons $n_s^{(b)}(B)$ as a function of the magnetic field strength. The used parameters are the same as those for the magnetoresistance shown in Fig. 10.

$$\sigma_{yy}^{\text{bound}}=\frac{e^2\tau}{m^*}\frac{2m^*}{\pi^2\hbar}\int_0^{k_c}[1-p(k_x,B)]v_y(k_x,E_F)dk_x$$

$$\equiv\sigma_0\frac{n_s^{(b)}(B)}{n_s}, \tag{31}$$

where the explicit form of the velocity component $v_y(k_x,E_F)$ is defined by Eq. (29):

$$v_y(k_x,E_F)=\frac{1}{m^*}\sqrt{2m^*(E_F+V_0)-4\hbar^2k_x^2}. \tag{32}$$

The quantity $p(k_x,B)$ is the probability that the Fermi state with wave number $|k_x|<k_c$ takes part in any of the available close orbits at given magnetic field B, i.e., it has the meaning of the magnetic breakdown probability. It has been determined numerically. Simultaneously with the calculation of $\sigma_{\alpha\beta}^{\text{close}}$ the times Δt_i spent by Fermi electrons within angle intervals $\Delta\phi_i$ have been established. The condition that the ratios of these times has to be the same as those at $B=0$ immediately leads to the probability values. This corresponds to the condition that the local areal density as well as velocity distribution are not changed by magnetic fields. Due to the formation of close orbits subsequent reflection events become correlated and $p(k_x,B)$ depends on $\omega_c\tau$. Some of the electrons having, in the classical sense large enough momentum along the $\hat{x}$ direction to escape from the well region, remain bounded because of the limited density of open orbits.

The resulting magnetoresistance ρ_{xx} as a function of the magnetic field for several values of the modulation amplitude V_0 is shown in Fig. 10. To stress the scaling of the breakdown peak positions with the parameters of the potential modulation we have used $B_{\text{crit}}=4V_0/(ea v_F)$ as the unit of the magnetic field strength ($v_F=\sqrt{2E_F/m^*}$). The resulting form of the magnetoresistance anomaly has the same qualitative features as that obtained in the limit of very weak modulation[16] where it has been argued that the breakdown peak is followed by a resistivity increase at higher magnetic fields due to the formation of Landau levels.

Opposite to some previously presented results,[5,12] represented in Fig. 10 by the approach of Beton *et al.*,[5] we have found that, for magnetic fields well above B_{crit}, instead of a rapid fall a positive magnetoresistance appears. This difference originates in the correlation between subsequent breakdown events which was completely ignored in the mentioned previous publications. As expected both approaches lead to the same result at very low magnetic fields, while at higher fields for which $\omega_c\tau\geqslant 1$ the correlation between subsequent reflections becomes important and results differ substantially.

The role of open trajectories is illustrated in Fig. 11 where the number of bound states $n_s^{(b)}(B)$ representing the conductivity contribution of open trajectories, Eq. (31), is plotted as a function of the magnetic field strength. This dependence represents the magnetic breakdown effect, i.e., the decreasing number of open trajectories with increasing magnetic field strength. The quantity $1-n_s^{(b)}(B)/n_s^{(b)}(0)$ may be interpreted as an effective breakdown probability, as seen from Eq. (31). For the Kronig-Penney model the fraction of bound states at $B=0$ is given by $n_s^{(b)}/n_s$ of Eq. (23).

VII. SUMMARY AND CONCLUDING REMARKS

The most pronounced effect of the periodic modulation is the formation of quasi-one-dimensional channels describing electrons which are bound within a single potential well. The number of these channels along the particular direction is approximately equal to the value of the parameter $q=2a\sqrt{m^*V_0}$. These states significantly influence the anisotropy of the velocity distribution and consequently the electronic transport. The perfect periodicity should lead to observable fluctuations of the conductivity as a function of the Fermi energy (see Fig. 7 and Fig. 8), i.e., of the electron concentration. This effect originates in the ordinary Bragg reflections due to the interference of electron waves scattered on different reflection planes. Note that the presented examples are close to the situations reached in the fabricated

superlattices. For example in the case with $q=6$ there are approximately 450 electrons per area a^2 for $E_F/V_0=4$. However, these fluctuations may be easily washed out even by weak inelastic scattering. Also, due to the sample nonuniformity they can be averaged out. However, if such a type of fluctuation for $B=0$ would be observed, it may be expected that in magnetic fields the effects due to the Hofstadter-type energy spectrum should appear.

Based on the knowledge of electron energy spectra, the low-field magnetoresistance can be evaluated, including the effect of the magnetic field into the electron dynamics controlled by the semiclassical equation of motion. To capture much of the additional ''high-field'' physics, the magnetic breakdown effect allowing electron transitions between different $\vec{k}$-space trajectories, i.e., between minibands, has to be taken into account. This effect gradually changes zero-field velocity distribution towards the classical distribution, which ignores interference effects (Bragg reflections) as well as the size quantization within potential well regions.

For the case of a strong unidirectional modulation, $q\geqslant 1$, the basic features of the low-field magnetoresistance anomaly have been established, assuming classical velocity distribution. It has been found that the typical strong positive magnetoresistance at very low fields is gradually suppressed by a decreasing number of electrons bounded within potential well regions. The position of the resulting breakdown peak, characterized by $B_{\rm crit}\sim V_0/a$, is controlled by the parameters of the potential modulation, the amplitude V_0, and the lattice constant a. The magnetoresistance peak is followed by a resistance increase at higher fields if the commensurability oscillations as well as Shubnikov–de Haas oscillations are smeared out. This positive magnetoresistance may be attributed to the nonvanishing number of bounded electrons due to the limited density of close orbits. The same features have been found by Menne and Gerhardts[18] by solving Boltzmann's equation for purely classical electrons.

The described form of the magnetoresistance anomaly might be affected by Bragg reflections at very low magnetic fields. In the case of strong modulation they lead to a substantial suppression of the zero-field conductivity, as shown in Fig. 7 and Fig. 8. This effect can be viewed as a special type of localization. The resulting miniband structure has tiny gaps, E_g, for which critical magnetic fields scale with aE_g^2. These gaps can be easily overcome by electrons at substantially weaker magnetic fields than $B_{\rm crit}$ of bounded electrons. Consequently it might be expected that the strong positive magnetoresistance due to the open trajectories located within potential well regions will be partly suppressed. In strongly modulated systems it can even be the origin of the often observed negative magnetoresistance at the lowest fields.[9–11]

The low-field magnetoresistance anomalies can also be affected by the anisotropy of the relaxation time which can be naturally expected in the case of the anisotropic velocity distribution. In the systems with dominating small-angle scattering the electron scattering between flat Fermi contour minisections can be suppressed. As a result, the highly conducting quasi-one-dimensional channels will dominate the electronic transport in strongly modulated systems. The magnetic breakdown effect allowing electron transition between different Fermi contour segments smears out the relaxation time anisotropy. This can also be the origin of the negative magnetoresistance in strongly modulated systems.[9]

ACKNOWLEDGMENTS

This work was supported in part by the Grant Agency of Czech Republic under Grant No. 202/94/1276 and by the NATO Collaborative Research Grant No. CRG921204.

*Present address: Technische Universität Cottbus, Karl-Marx-Strasse 17, D-03044 Cottbus, BRD.

[1] For reviews see C. W. Beenakker and H. van Houten, in *Quantum Transport in Semiconductor Nanostructures*, edited by H. Ehrenreich and D. Turnbull, Solid State Physics Vol. 44 (Academic Press, Boston, 1991); D. K. Ferry, Prog. Quantum Electron. **16**, 251 (1992); W. Hansen, J. P. Kotthaus, and U. Merkt, in *Semiconductors and Semimetals*, edited by R. K. Willardson, A. C. Beer, and E. P. Weber (Academic, San Diego, 1992), Vol. 35.

[2] D. Weiss, K. v. Klitzing, K. Ploog, and G. Weimann, Europhys. Lett. **8**, 179 (1989).

[3] R. R. Gerhardts, D. Weiss, and K. von Klitzing, Phys. Rev. Lett. **62**, 1173 (1989).

[4] R. W. Winkler, J. P. Kotthaus, and K. Ploog, Phys. Rev. Lett. **62**, 1177 (1989).

[5] P. H. Beton, E. S. Alves, P. C. Main, L. Eaves, M. W. Dellow, M. Henini, O. H. Hughes, S. P. Beaumont, and C. D. W. Wilkinson, Phys. Rev. B **42**, 9229 (1990).

[6] R. W. Stark, Phys. Rev. **135** A1698 (1964).

[7] L. M. Falicov and P. R. Sievert, Phys. Rev. **138**, A88 (1965).

[8] R. W. Stark and L. M. Falicov, Prog. Low-Temp. Phys. **5**, 235 (1967).

[9] G. Müller, P. Středa, D. Weiss, K. von Klitzing, and G. Weimann, Phys. Rev. B **50**, 8938 (1994).

[10] J. Takahara, T. Kakuta, T. Yamashiro, Y. Takagaki, T. Shiokawa, K. Gamo, S. Namba, S. Takaoka, and K. Murase, Jpn. J. Appl. Phys. **30**, 243 (1991).

[11] E. S. Alves, P. H. Beton, M. Henini, L. Eaves, P. C. Main, O. H. Hughes, G. A. Toombs, S. B. Beaumont, and C. D. W. Wilkinson, J. Phys. Condens. Matter **1**, 8257 (1989).

[12] P. Středa, J. Kučera, and J. van de Konijnenberg, Phys. Scr. **T39**, 162 (1991).

[13] E. I. Blount, Phys. Rev. **126**, 1636 (1962); A. B. Pippard, Proc. R. Soc. London, Ser. A **270**, 1 (1962); J. R. Reitz, J. Phys. Chem. Solids **25**, 53 (1964).

[14] C. W. J. Beenakker, Phys. Rev. Lett. **62**, 2020 (1989).

[15] P. Vasilopoulos and F. M. Peeters, Phys. Rev. Lett. **63**, 2120 (1989).

[16] P. Středa and A. H. MacDonald, Phys. Rev. B **41**, 11 892 (1990).

[17] P. H. Beton, M. W. Dellow, P. C. Main, E. S. Alves, L. Eaves, S. P. Beaumont, and C. D. W. Wilkinson, Phys. Rev. B **43**, 9980 (1991).

[18] R. Menne and R. R. Gerhardts, in *Proceedings of the 12th International Conference on Applied High Magnetic Fields, Würzburg, 1996* (World Scientific, Singapore, in press).

[19] R. G. Chambers, Proc. Phys. Soc. London, Ser. A **81**, 877 (1963). See also N. W. Ashcroft and N. D. Mermin, *Solid State Physics* (Saunders College, Philadelphia, 1976).